Available online at www.sciencedirect.com

ScienceDirect

Ceramics International 40 (2014) 2723–2729

CERAMICS INTERNATIONAL

www.elsevier.com/locate/ceramint

Role of interface on electrical conductivity of carbon nanotube/alumina nanocomposite

Soumya Sarkar[a], Probal Kr. Das[a,*]

[a]Non-oxide Ceramics & Composites Division, CSIR-Central Glass & Ceramic Research Institute (CSIR-CG&CRI), Kolkata 700032, India

Received 12 August 2013; received in revised form 10 October 2013; accepted 11 October 2013
Available online 21 October 2013

Abstract

Interface of multiwalled carbon nanotube (MWCNT)/alumina (Al_2O_3) nanocomposites have been studied using TEM. At low sintering temperature (T_{sin} = 1500 °C), a 3–5 nm thick amorphous interface region was noticed. Nanocomposite sintered at 1700 °C possessed a well-defined graphene layer coating on matrix grains as the interface between CNT and Al_2O_3. A mechanism of such layered interface formation has been proposed. No traceable chemical reaction product was observed at the interface even after sintering at 1700 °C. It was noticed that while DC electrical conductivity (σ_{DC}) of 1500 °C sintered 2.4 vol% MWCNT/Al_2O_3 nanocomposite was only ~0.02 S/m, it raised to ~21 S/m when sintering was done at 1700 °C. Such 10^3 times increase in σ_{DC} of present nanocomposite at a constant CNT loading was not only resulted from the exceptionally high electron mobility of CNT but the well-crystallized graphene interface on insulating type Al_2O_3 grains also significantly contributed in the overall increase of electrical performance of the nanocomposite, especially, when sintering was done at 1700 °C.

Keywords: B. Electron microscopy; B. Interfaces; B. Nanocomposites; C. Electrical conductivity

1. Introduction

In composites, optimum interface performance is essential since it decides how effectively applied load (mechanical), electron (electrical/electronic) and phonon (thermal) transfer occurs among its constituents [1]. Therefore, interface characterization is indispensable to establish the exact structure-property relationship in composites. CNT reinforced ceramic matrix nanocomposites viz. CNT/Al_2O_3, CNT/Si_3N_4, CNT/ZrO_2, CNT/SiC, CNT/SiO_2-ZnO are not exception in this regard [2–6]. Although, many reports are available on property evaluation of the most ancient, economic and versatile ceramic i.e. Al_2O_3 reinforced with CNT [7–13], limited work has been performed on CNT/Al_2O_3 interface characterization [7–8,13–14]. Further, most of these reports dealt with structural integrity of CNT in sintered nanocomposites and position of nanotubes in matrix phase (i.e. within, outside or at grain boundary position). The primary aim of present work was to study the interface/interaction region of pressureless sintered CNT/Al_2O_3 nanocomposites and changes in interface nature with increasing T_{sin} using TEM. Finally, correlation between observed CNT/Al_2O_3 interface and σ_{DC} of present nanocomposites was analyzed.

2. Experimental procedures

2.1. Raw material and sample preparation

Multiwalled CNT (MWCNT: *Shenzhen NTP*, *China*, > 95 wt% pure) and Al_2O_3 powder (*Almatis*, *ACC Ltd.*, *India*, 99.8 wt% pure) were used as raw materials [12]. The nanocomposite fabrication procedure can be found elsewhere [12]. In brief, nanocomposite powder mixtures were prepared by wet-mixing of as-received dispersed raw materials followed by drying and sieving. Sintering was done in a graphite resistance heating furnace (*1000-4560-FP20*; *Thermal Technology Inc. U.S.A.)* under static Argon (Ar: 35–70 kPa) (Table 1).

*Corresponding author. Tel.: +91 33 2473 3469/76/77/96; fax: +91 33 2473 0957.
E-mail addresses: probal@cgcri.res.in, probalkdas@rediffmail.com (P.Kr. Das).

0272-8842/$ - see front matter © 2013 Elsevier Ltd and Techna Group S.r.l. All rights reserved.
http://dx.doi.org/10.1016/j.ceramint.2013.10.049

Table 1
Batch details, sintering schedule, nomenclature and theoretical density of studied specimens.

Batch id	CNT (wt%)	Sintering schedule	Sintered as	Specimen id	TD (g/cc)
A	0.00	1500 °C/2 h./Ar	Pellet	*A15*	3.970
		1600 °C/2 h/Ar	Pellet	*A16*	
		1700 °C/2 h/Ar	Pellet	*A17*	
B	0.07	1500 °C/2 h/Ar	Pellet	*B15*	3.967
		1600 °C/2 h/Ar	Pellet	*B16*	
		1700 °C/2 h/Ar	Pellet	*B17*	
C	0.13	1500 °C/2 h/Ar	Pellet	*C15*	3.963
		1600 °C/2 h/Ar	Pellet	*C16*	
		1700 °C/2 h/Ar	Pellet	*C17*	
D	0.27	1500 °C/2 h/Ar	Pellet	*D15*	3.957
		1600 °C/2 h/Ar	Pellet	*D16*	
		1700 °C/2 h/Ar	Pellet	*D17*	
E	0.54	1500 °C/2 h/Ar	Pellet	*E15*	3.944
		1600 °C/2 h/Ar	Pellet	*E16*	
		1700 °C/2 h/Ar	Pellet	*E17*	
F	1.09	1500 °C/2 h/Ar	Pellet	*F15*	3.917
		1600 °C/2 h/Ar	Pellet	*F16*	
		1700 °C/2 h/Ar	Pellet	*F17*	
G	35.00	1500 °C/2 h/Ar	Powder	*G15*	2.771
		1600 °C/2 h/Ar	Powder	*G16*	
		1700 °C/2 h/Ar	Powder	*G17*	

2.2. Interface characterization

For interface observations, sintered nanocomposites were observed through TEMs (*Tecnai G²30ST* and *Tecnai G²20ST*, *FEI Company*, *The Netherlands*). It may be seen from Table 1 that beside bulk nanocomposites containing 0.07–1.09 wt% CNT (i.e. batch ♯'*A*'–'*F*'), nanocomposite powder containing 35 wt% MWCNT (i.e. batch '*G*') was also heat-treated at the sintering temperatures. Purpose of using such a high nanotube concentration was to minimize chances of structural damage of CNTs and interface regions in pelletized nanocomposites caused by ultrasonic slicing, dimple grinding and ion-milling steps required for TEM bulk specimen preparation and to raise the probability of finding CNT/Al_2O_3 interface due to significantly high CNT content.

2.3. Electrical property measurement

Room temperature (*RT*) σ_{DC} of pelletized MWCNT/Al_2O_3 nanocomposites and pure Al_2O_3 was measured by standard 2-probe method using a *2400 Sourcemeter*, *Keithley Instrument Inc.*, *U.S.A*. Results were correlated with the nature of interface formed in the nanocomposites.

3. Results and discussions

3.1. Physical properties of the sintered specimens

Plot of relative density (*RD*) values of all the specimens is shown in Fig. 1. The *RD* values were calculated using the theoretical density (*TD*) values of corresponding specimens given in Table 1. Theoretical density of each of the specimens were calculated using *Rule of Mixture* taking $\rho_{Al2O3}=3.97$ g/cc and $\rho_{MWCNT}=1.775$ g/cc [11,13]. Densities of sintered bulk specimens were evaluated using the *Archimedes water immersion* technique and that for specimen '*G*' were evaluated by standard *Tapping* method. Detailed discussion on physical properties and microstructure of present nanocompostes can be found elsewhere [11,13].

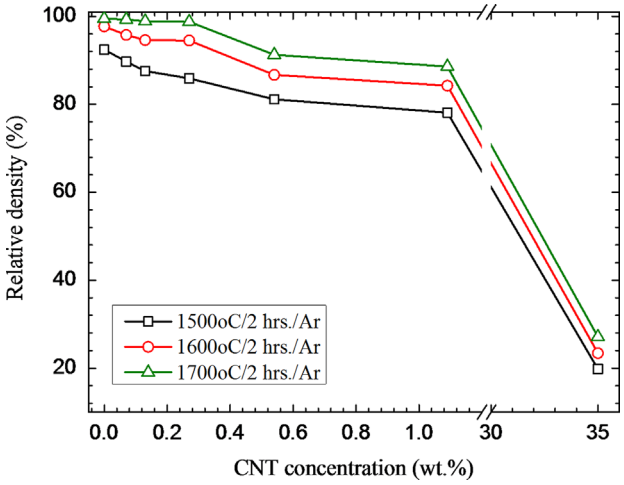

Fig. 1. Physical properties of the studied specimens.

3.2. Interface analyses of the sintered specimens

TEM images of as-received MWCNTs indicated presence of tubes of different diameters having partialy alligned graphene layers and apperently smooth external surfaces (Fig. 2(a–b)). However, in certain cases (Fig. 2(b)), a very thin layer was noticed on the externatl wall of CNTs that possibly came from residual amorphous carbon (3–5 wt%) and/or other impurities present in as-received MWCNT [15]. Except Fig. 2(a–b), interested readers can found additional TEM images of as-received MWCNTs in our earlier communications [15–16]. TEM image of *D15* confirmed structural stability of CNT after sintering at 1500 °C for 2 h in Argon (Fig. 3(a)). Bamboo structured CNTs and attachment of nanotubes with Al_2O_3 grains were also observed (Fig. 3(a)). Interface in *D15* had no well-defined crystalline pattern; it was rather amorphous in nature having thickness of 3–5 nm (Fig. 3(b)). Presence of CNT agglomerates at *intergranular* pores was noticed in *F17* (Fig. 4(a)). Interestingly, at higher magnification, existence of certain reaction zone was observed in *F17* through which CNTs were attached with the matrix grains (Fig. 4(b)). Thus, sintering at 1700 °C possibly helped in formation of a distinct interface in the nanocomposites to hold CNT and Al_2O_3 grains together and played a significant role in property enhancement of studied specimens [12]. To further confirm this, sintered nanocomposite powder (batch '*G*') was studied using TEM. Fig. 5(a) shows that in *G15*, CNTs were attached with Al_2O_3 grains by the so-called *pinning* action [8,10,14] and there was no interface formed between filler and matrix. Fig. 5(b) shows *side-by-side* attachment of CNT and Al_2O_3 in *G15* without any traceable chemical reaction product at the boundary. Similarly, in *G16*, penetration of survived CNTs in matrix was noticed (Fig. 6(a)). Surprisingly, a graphene layer coating of a few nanometer thicknesses and having interlayer spacing of ~0.34 nm was found around the matrix grains after sintering at 1600 °C (Fig. 6(b)). Finally, after sintering at 1700 °C of the nanocomposite powder, TEM study confirmed characteristic existence of the graphene layer encapsulation of the matrix grains that acted as interface between CNT and Al_2O_3 (Fig. 7 (a–b)). A possible sequence of such layered interface formation in this nanocomposite is shown in Fig. 8. It has been reported that at temperature > 1500 °C in Argon, splitting of external graphene layers of MWCNTs from either highly strained regions or defects is possible [16]. Under high temperature and/or pressure, such deformed/splitted nanotubes are tending to form different caged nano-structures [17]. Further, as reported by Sarkar and Das [15–16], formation of various nano-structures or distinct graphene layers was more favorable

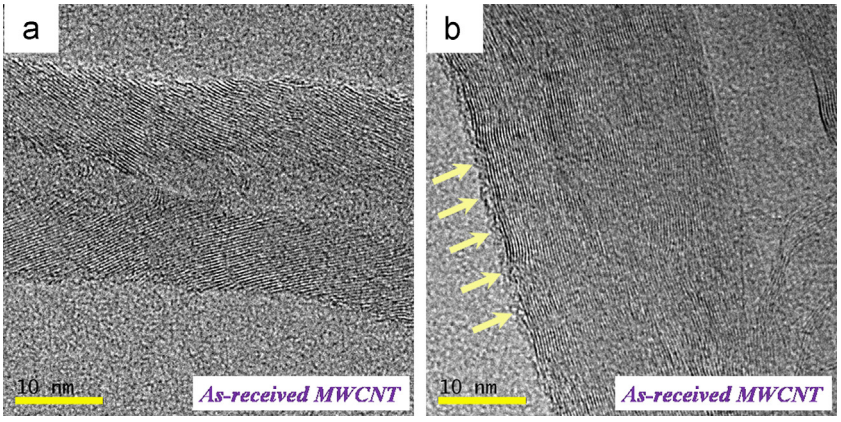

Fig. 2. TEM images of as-received MWCNT showing partially aligned graphene layers (a) in a thin CNT and (b) thick CNT having very thin layer (indicated by pointed arrows) on the external surface possibly of residual amorphous carbon or other impurities; scale bar: 10 nm.

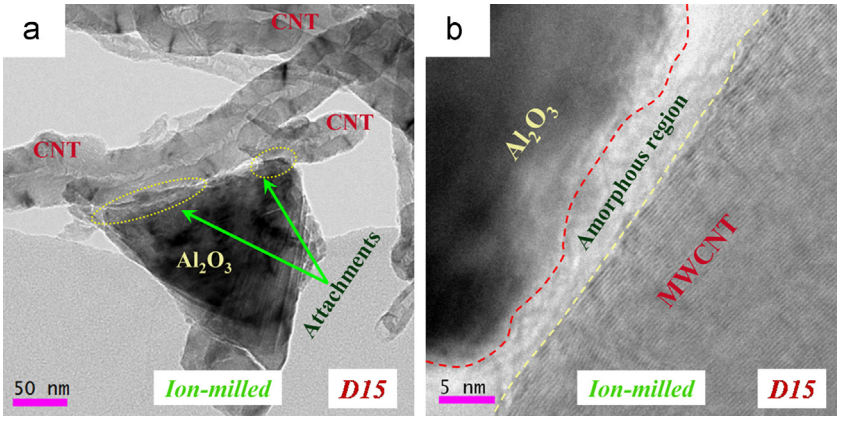

Fig. 3. TEM images of *D15* showing: (a) attachment of CNTs with Al_2O_3 grains; scale bar: 50 nm, and (b) amorphous interface; scale bar: 5 nm.

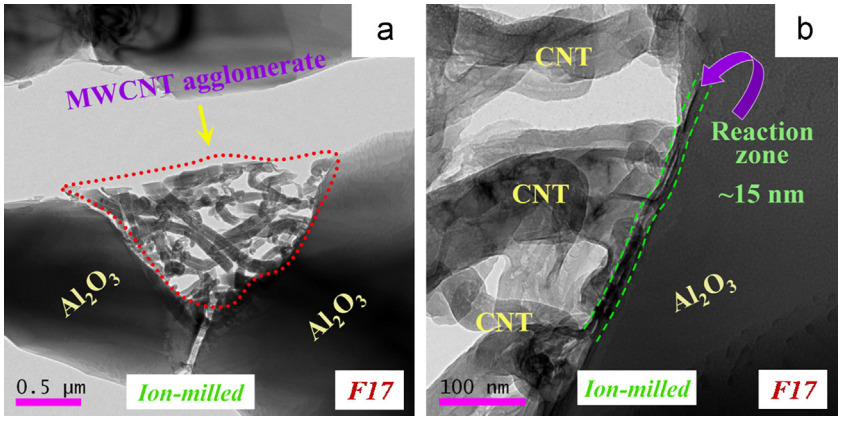

Fig. 4. TEM images of *F17* showing (a) presence of nanotube agglomerate at *intergranular* pore; scale bar: 0.5 μm and (b) interaction zone; scale bar: 100 nm.

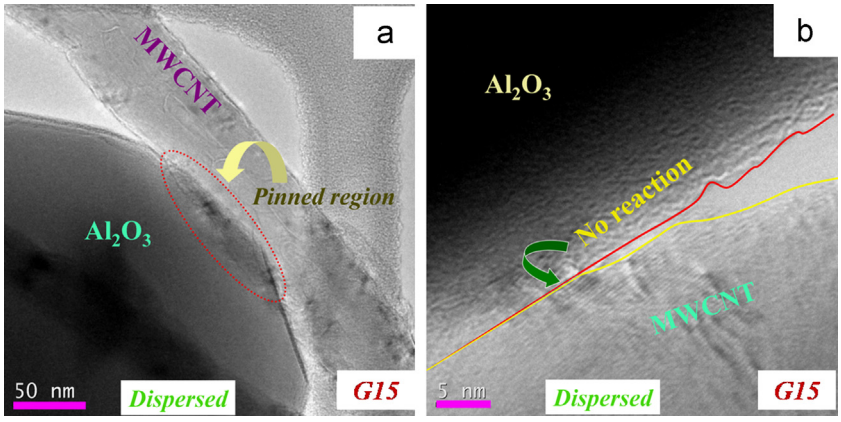

Fig. 5. TEM images of *G15* showing (a) *pinning* of Al_2O_3 grains by CNT; scale bar: 50 nm and (b) *side-by-side* attachment of CNT-Al_2O_3; scale bar: 5 nm.

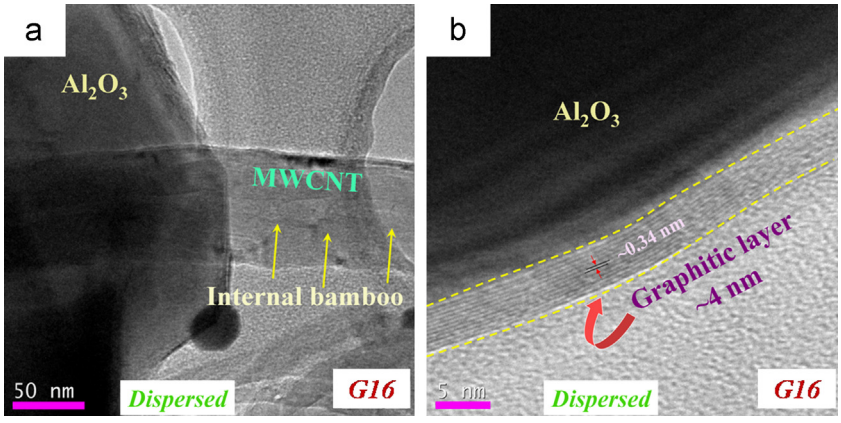

Fig. 6. TEM images of *G16* showing (a) penetrated CNT in matrix grain; scale bar: 50 nm, and (b) formation of graphitic layer on Al_2O_3; scale bar: 5 nm.

in singlewalled CNTs (SWCNTs) than MWCNTs when exposed to high temperature (~1800 °C) in inert atmosphere. In SWCNT, splitting of only a single graphene layer entirely damaged the tubular morphology and transformed into other polygonal nano-shapes by stacking of such splitted layers from many such SWCNTs at high temperatures (~1800 °C). On contrary, in MWCNTs, due to the presence of interwall *van der Walls* attractive forces and possibly certain cross-linking effects, the splitted layers did not completely detach from the parent nanotube and formed nano-scale corrugation on the external wall of heat-treated MWCNTs [16]. In present case, pressure on CNTs might arouse from the overall volume shrinkage of consolidating nanocomposites. Thus, once the strained/defective layers splitted from external wall of MWCNTs during sintering they retreated in the opposite direction for strain relaxation and surrounding growing Al_2O_3 grains squeezed the splitted graphene layers within them and by the action of heat and pressure, the squeezed

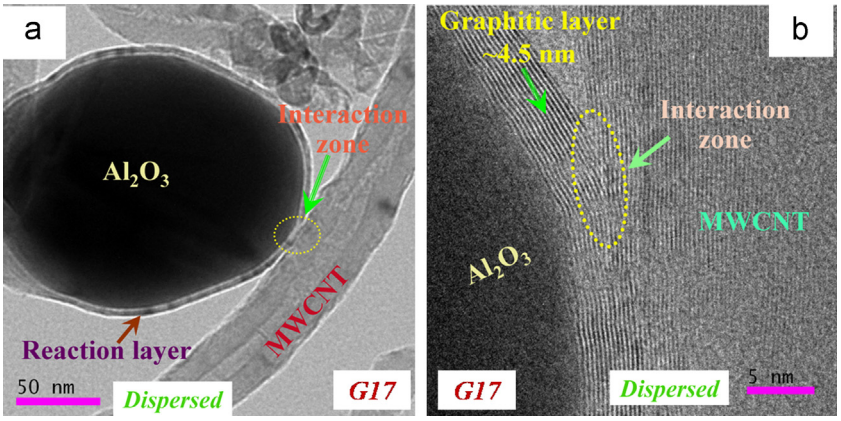

Fig. 7. TEM images of *G17* showing (a) attachment of CNTs with Al_2O_3 grain through graphene layer encapsulation; scale bar: 50 nm and (b) HRTEM image of the layered interface; scale bar: 5 nm.

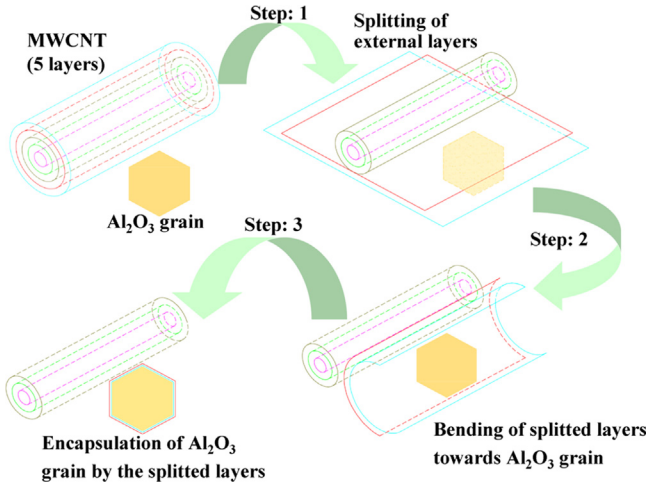

Fig. 8. Schematic of proposed mechanism of layered interface formation in CNT/Al_2O_3 nanocomposites.

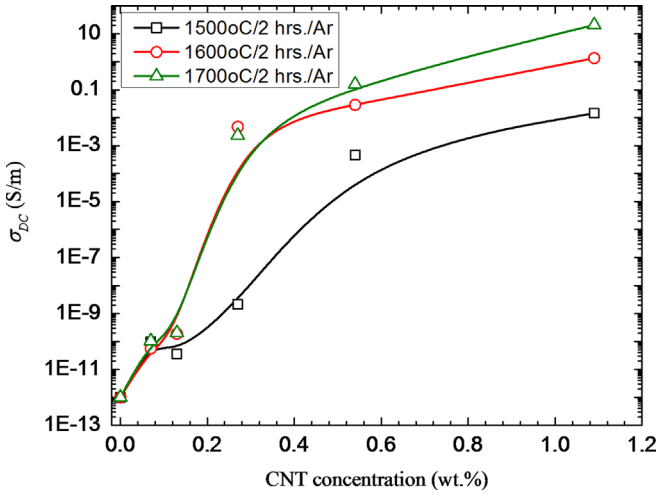

Fig. 9. Plot RT σ_{DC} versus CNT concentration of pelletized nanocomposites.

layers ultimately deposited on the surface of Al_2O_3 grains to create the thin graphene layer encapsulation. By this process, Al_2O_3 grains attached with a rather narrow diameter CNT through this layer, especially, at higher T_{sin} (Fig. 8). The graphene encapsulation not only provided an interface between CNT and Al_2O_3, but also stopped growth of encapsulated Al_2O_3 grains resulting in finer grain size in nanocomposites over pure Al_2O_3 sintered under identical condition. During TEM studies, no Al–O–C compound was detected in these nanocomposites as reported by others [8,13].

3.3. Electrical properties of the sintered specimens

RT σ_{DC} values of pelletized specimens sintered at three T_{sin}s are shown in Fig. 9. σ_{DC} of pure Al_2O_3 at *RT* was taken as 10^{-12} S/m [18]. It may be seen from the figure that increasing CNT content in highly resistive Al_2O_3 rendered significant enhancement in σ_{DC}, especially, at CNT loading ≥ 0.6 vol%. Furthermore, with increase in T_{sin}, the so-called *percolation threshold* i.e. conductive network of CNT was decreased from 1.2 vol% MWCNT loading for 1500 °C sintered specimens to 0.6 vol% MWCNT for 1600° and 1700 °C sintered nanocomposites. Such lowering of percolation threshold on increasing T_{sin} was aroused due to the fact that at low T_{sin}, shrinkage of nanocomposites was less and thus, desired interconnected network of highly conducting CNTs was only achieved for specimens containing 1.2 or 2.4 vol% CNT. Since, 1.2 or 2.4 vol% CNT/Al_2O_3 nanocomposites characteristically contained agglomerated CNTs along the matrix grain boundaries, even at low shrinkage, these specimens exhibited highly conducting nature compared to pure Al_2O_3. On the other hand, sintering at higher temperatures (i.e. 1600 or 1700 °C) resulted in further shrinkage of nanocomposites leading to the formation of desired percolating CNT network in nanocomposites containing ≥ 0.6 vol% CNT by reducing the spacing among the tubes and ensured enhanced tunneling effect of electrons through individual CNTs or bundles. While an abrupt increase in σ_{DC} from $\sim 10^{-12}$ S/m for pure Al_2O_3 to 10^{-4} S/m for *E15* specimen was observed among the 1500 °C sintered specimens, among 1600 and 1700 °C sintered specimens, *percolation* was noticed at 0.6 vol% CNT loading and σ_{DC} changed from $\sim 10^{-12}$ S/m for pure Al_2O_3 to $\sim 10^{-3}$ S/m for the nanocomposite (Fig. 9). The low percolation concentration

(i.e. ≥ 0.6 vol% CNT) obtained for present CNT/Al_2O_3 nanocomposites were consistent with the previous reports on CNT/ceramic nanocomposites and was attributed to high aspect ratio of present MWCNTs ($83 \leq l/d \leq 150$), high electrical conductivity $\approx 1.85 \times 10^3$ S/m and current density (10^7 A/cm^2) along tube axis of undamaged MWCNTs [18–25]. Among all the specimens, the highest σ_{DC} at *RT* was obtained for batch '*F*' sintered nanocomposites ($^{F15}\sigma_{DC}$=0.0146 S/m; $^{F16}\sigma_{DC}$=1.36 S/m and $^{F17}\sigma_{DC}$=21 S/m). Now, the question is that why σ_{DC} of *F17* was found to be 10^3 times higher than that of *F15* although both of the specimens contained 2.4 vol% nanotube? The reasons are the following:

i. Increased densification at higher T_{sin}, ensured better connectivity among the nanotubes and resulted in higher σ_{DC} at constant CNT loading.
ii. In a recent communication, Liu et al. [6] reported that reaction between CNT and ZnO helped in effective removal of residual amorphous carbon from the nanotubes and created higher oxygen vacancies in ZnO during sintering of a CNT/SiO_2-ZnO nanocomposite and drastically enhanced the σ_{DC} of the nanocomposite over pure SiO_2. In a similar way, in present study high temperature sintering might helped in amorphous carbon removal from MWCNTs and rendered better connectivity among the tubes resulting in increased σ_{DC} of the nanocomposites.
iii. Formation of a well-crystallized and a few layer thick graphene interface on insulating Al_2O_3 grains at higher T_{sin} rendered exceptional increase in σ_{DC} to the high temperature (≥ 1600 °C) sintered nanocomposites even at constant CNT loading. This was due to the fact that carrier mobility, current density in graphene nano-ribbons that resembles the interface formed in present nanocomposite can go up to 2×10^5 cm^2/V-s and 10^{11}–10^{13} A/m^2 which are comparable or even better than MWCNT [19,26–30]. Since, attachment of reinforcing nanotubes with the graphene interface was found to be much better in 1700 °C sintered nanocomposites (Fig. 4(b) and clarified in Fig. 7(a and b)), σ_{DC} also increased 10^3 times over *F15* containing an amorphous interface (Fig. 3(b)).

4. Conclusions

At low T_{sin}, pressureless sintered CNT/Al_2O_3 nanocomposite possessed an amorphous interface. Attachment of CNT with Al_2O_3 grains was primarily a result of *pinning* by nanotubes. At 1700 °C, a thin graphene layer encapsulation was formed on Al_2O_3 grains that provided a prominent interface between CNT and Al_2O_3 and helped in grain refining of sintered nanocomposites. The layered encapsulation was formed by splitting of strained/defective external graphene layers of MWCNTs at high T_{sin} (>1500 °C) followed by bending towards and squeezing by the neighboring Al_2O_3 grains to form the close structure. The graphene interface in 1700 °C sintered nanocomposites contributed notably in overall increase of σ_{DC} by 10^3 times over the low temperature sintered specimens by minimizing the effect of insulating matrix and providing better connecting path among the nanotubes free from amorphous carbon and other impurities for electron transport.

Acknowledgments

The authors wish to acknowledge the Director, CSIR-CG&CRI, India for his permission to publish this work. They also thank the personnel of Electron Microscopy Section of CSIR-CG&CRI, India for helping in TEM study. First author acknowledges financial support of the Council of Scientific and Industrial Research (CSIR), India.

References

[1] A.G. Evans, D.B. Marshall, Mechanical behavior of ceramic matrix composites, in: K.S. Mazdiyasni (Ed.), Fiber reinforced Ceramic Composites: Materials, Processing, and Technology, Noyes Publications, Park Ridge, New Jersey, USA, 1990.
[2] J. Echeberria, N. Rodrı´guez, J. Vleugels, K. Vanmeensel, A. Reyes-Rojas, A. Garcia-Reyes, C. Domı´nguez-Rios, A. Aguilar-Elgue´zabal, M.H. Bocanegra-Bernal, Hard and tough carbon nanotube-reinforced zirconia-toughened alumina composites prepared by spark plasma sintering, Carbon 50 (2012) 706–717.
[3] X. Liu, X. Yin, G. Zheng, Y. Liu, L. Kong, Q. Li, X. Yuan, In-situ formation of carbon nanotubes in pyrolytic carbon–silicon nitride composite ceramics, Ceram. Int. Available online 18 June 2013, http://dx.doi.org/10.1016/j.ceramint.2013.06.035.
[4] J. Yi, T. Wang, Z. Xie, W. Xue, Zirconia-based nanocomposite toughened by functionalized multi-wall carbon nanotubes, J. Alloy. Compd. 581 (2013) 452–458.
[5] J. Hu, S. Dong, X. Zhang, H. Zhou, B. Wu, Z. Wang, P. He, L. Gao, Process and mechanical properties of carbon/carbon–silicon carbide composite reinforced with carbon nanotubes grown in situ, Compos. Part A: Appl. Sci. Manuf. 48 (2013) 73–81.
[6] Y. Liu, X. Yin, L. Kong, X. Liu, F. Ye, L. Zhang, L. Cheng, Electromagnetic properties of SiO_2 reinforced with both multi-wall carbon nanotubes and ZnO particles, Carbon 64 (2013) 541–544.
[7] M. Estili, A. Kawasaki, H. Sakamoto, Y. Mekuchi, M. Kuno, T. Tsukada, The homogeneous dispersion of surfactantless, slightly disordered, crystalline, multiwalled carbon nanotubes in α-alumina ceramics for structural reinforcement, Acta Mater. 56 (2008) 4070–4079.
[8] I. Ahmad, M. Unwin, H. Cao, H. Chen, H. Zhao, A. Kennedy, Y.Q. Zhu, Multi-walled carbon nanotubes reinforced Al_2O_3 nanocomposites: mechanical properties and interfacial investigations, Compos. Sci. Technol. 70 (2010) 1199–1206.
[9] K. Lee, C.B. Mo, S.B. Park, S.H. Hong, Mechanical and electrical properties of multiwalled CNT-alumina nanocomposites prepared by a sequential two-step processing of ultrasonic spray pyrolysis and spark plasma sintering, J. Am. Ceram. Soc. 94 (2011) 3774–3779.
[10] S. Bi, G. Hou, X. Su, Y. Zhang, F. Guo, Mechanical properties and oxidation resistance of α−alumina/multi-walled carbon nanotube composite ceramics, Mater. Sci. Eng. A 528 (2011) 1596–1601.
[11] S. Sarkar, P.K. Das, Temperature and load dependent mechanical properties of pressureless sintered carbon nanotube/alumina nanocomposites, Mater. Sci. Eng. A 531C (2012) 61–69.
[12] S. Sarkar, P.K. Das, Microstructure and physicomechanical properties of pressureless sintered multiwalled carbon nanotube/alumina nanocomposites, Ceram. Int. 38 (2012) 423–432.
[13] S. Sarkar, P.K. Das, Statistical analysis of mechanical properties of pressureless sintered multiwalled carbon nanotube/alumina nanocomposites, Mater. Chem. Phys. 137 (2012) 511–518.
[14] I. Ahmad, H. Cao, H. Chen, H. Zhao, A. Kennedy, Y.Q. Zhu, Carbon nanotube toughened aluminium oxide nanocomposite, J. Eur. Ceram. Soc. 30 (2010) 865–873.

[15] S. Sarkar, P.K. Das, Thermal and structural stability of single- and multi-walled carbon nanotubes up to 1800 °C in Argon studied by Raman spectroscopy and transmission electron microscopy, Mater. Res. Bull. 48 (2013) 41–47.
[16] S. Sarkar, P.K. Das, S. Bysakh, Effect of heat treatment on morphology and thermal decomposition kinetics of multiwalled carbon nanotubes, Mater. Chem. Phys. 125 (2011) 161–167.
[17] M. Zhang, D.W. He, L. Ji, B.Q. Wei, D.H. Wu, X.Y. Zhang, Y.F. Xu, W. K. Wang, Microstructural changes in carbon nanotubes induced by annealing at high pressure, Carbon 37 (1999) 657–662.
[18] G.-D. Zhan, A.K. Mukherjee, Carbon nanotube reinforced alumina-based ceramics with novel mechanical, electrical and thermal properties, Int. J. Appl. Ceram. Technol. 1 (2) (2004) 161–171.
[19] Y. Ando, X. Zhao, H. Shimoyama, G. Sakai, K. Kaneto, Physical properties of multiwalled carbon nanotubes, Int. J. Inorganic Mater. 1 (1999) 77–82.
[20] K. Ahmad, W. Pan, Dramatic effect of multiwalled carbon nanotubes on the electrical properties of alumina based ceramic nanocomposites, Compos. Sci. Technol. 69 (2009) 1016–1021.
[21] K. Ahmad, W. Pan, S.-L. Shi, Electrical conductivity and dielectric properties of multiwalled carbon nanotube and alumina composites, Appl. Phys. Lett. 89 (2006) 133122.
[22] F. Inam, H. Yan, D.D. Jayaseelan, T. Peijs, M.J. Reece, Electrically conductive alumina-carbon nanocomposites prepared by spark plasma sintering, J. Eur. Ceram. Soc. 30 (2010) 153–157.
[23] K. Lee, C.B. Mo, S.B. Park, S.H. Hong, Mechanical and electrical properties of multiwalled CNT-alumina nanocomposites prepared by a sequential two-step processing of ultrasonic spray pyrolysis and spark plasma sintering, J. Am. Cream. Soc. 94 (11) (2012) 3774–3779.
[24] L. Kumari, T. Zhang, G.H. Du, W.Z. Li, Q.W. Wang, A. Datye, K. H. Wu, Synthesis, microstructure and electrical conductivity of carbon nanotube-alumina nanocomposites, Ceram. Int. 35 (2009) 1775–1781.
[25] M. Poorteman, M. Traianidis, G. Bister, F. Cambier, Colloidal processing, hot pressing and characterisation of electroconductive MWCNT-alumina composites with compositions near the percolation threshold, J. Eur. Ceram. Soc. 29 (2009) 669–675.
[26] W.Y. Jang, N.N. Kulkarni, C.K. Shih, Z. Yao, Electrical characterization of individual carbon nanotubes grown in nanoporous anodic alumina templates, Appl. Phys. Lett. 84 (7) (2004) 1177–1179.
[27] L. Zeng, X.Y. Liu, G. Du, J.F. Kang, R.Q. Han, Evaluation of mobility in graphene nanoribbons including line edge roughness scattering, In: SISPAD 2009, San Diego, CA, 2009, pp. 1–4.
[28] A. Behnam, A.S. Lyons, M.-H. Bae, E.K. Chow, S. Islam, C. M. Neumann, E. Pop, Transport in nanoribbon interconnects obtained from graphene grown by chemical vapor deposition, Nano Lett. 12 (2012) 4424–4430.
[29] K.-J. Lee, A.P. Chandrakasan, J. Kong, Breakdown current density of CVD-grown multilayer graphene interconnects, IEEE Electron. Device Lett. 32 (2011) 557–559.
[30] K.S. Novoselov, V.I. Falko, L. Colombo, P.R. Gellert, M.G. Schwab, K. Kim, A roadmap for graphene, Nature 490 (2012) 192–200.